Directional analysis of measured 60 GHz indoor radio channels using SAGE

Gustafson, Carl; Tufvesson, Fredrik; Wyne, Shurjeel; Haneda, Katsuyuki; Molisch, Andreas F

Published in:
[Host publication title missing]

DOI:
10.1109/VETECS.2011.5956639

2011

Directional Analysis of Measured 60 GHz Indoor Radio Channels using SAGE

Carl Gustafson*, Fredrik Tufvesson*, Shurjeel Wyne†, Katsuyuki Haneda‡ and Andreas F. Molisch§
*Department of Electrical and Information Technology, Lund University, Sweden,
†COMSATS Institute of Information Technology, Islamabad, Pakistan,
‡Department of Radio Science and Engineering, Aalto University School of Science and Technology, Finland,
§Dept. of Electrical Engineering, University of Southern California, Los Angeles, CA, USA

***Abstract*—Directional properties of the radio channel are of high importance for the development of reliable wireless systems operating in the 60 GHz frequency band. Using transfer functions measured from 61 to 65 GHz in a conference room we have extracted estimates of the multi-path component parameters using the SAGE algorithm. In the paper we compare results for line-of-sight (LOS) scenarios and the corresponding non-line-of-sight (NLOS) scenarios and present values of the direction spread at the Tx and the Rx.**

I. Introduction

Significant research activity is currently being undertaken to design next generation high-speed wireless systems operating in the 60 GHz band, in particular for Gbit/s transmission over short distances. Several standards (IEEE 802.15.3c, IEEE 802.11ad) are emerging, and products are available on the market. The 60 GHz band is of interest mainly due to the large bandwidth of at least 5 GHz that is available world-wide. However, the attenuation of radio waves at 60 GHz is very high, for several reasons: (i) the free-space pathloss is proportional to the square of the carrier frequency (assuming constant-gain antennas), and thus much higher than for the 2 and 5 GHz bands commonly used today [1] (ii) the dimensions of physical objects in a room are typically large in relation to the wavelength of 5 mm, resulting in sharp shadow zones and (iii) transmission through obstacles such as walls is low. The challenges related to these propagation characteristics needs to be addressed in order to be able to establish a reliable communication link in the 60 GHz band. One possible solution is to use beamforming where the individual phases of the antenna elements in an array are electronically controlled to achieve a suitable array pattern. Using beam switching [2], beamforming can be designed to direct the beam towards different directions depending on the situation. For instance, if the LOS is blocked, the beam can be steered towards a direction where a strong first order reflection is available.

For the above reasons, the directional properties of the 60 GHz channel is of high importance, as is reflected by the previous work on this topic. In [4], the 60 GHz channel was measured for typical indoor environments using a 1×4 patch array antenna and the SAGE algorithm was used to estimate the direction of arrival (DOA) in azimuth. In [3], highly directional antennas were mechanically steered in order to determine the DOA characteristics for several different environments, including typical building hallways and small to medium sized rooms. The study confirmed that the majority of the components in the LOS scenario could be determined from ray tracing techniques. In this paper, we use the SAGE algorithm and a virtual array setup to analyze the directional properties of measured channels in a conference room. We compare the results for different LOS scenarios with the corresponding NLOS scenarios. The results include estimates of the direction of departure and direction of arrival in both azimuth and elevation, as well as measures of the direction spread.

A. The IEEE802.15.3c channel model

A complete channel model for mm-wave systems was developed and standardized by the IEEE802.15.3c working group. It supports several different scenarios, including office, desktop and library scenarios [5]. The angular characteristics of the channel is only considered at the Tx side. A particular simplification is that for desktop, office and library scenarios, the NLOS model is derived from the LOS model by removing the LOS component. In this paper, we investigate by measurement whether such a simplification is a good approximation to reality; i.e., we compare the directional estimates of the LOS scenarios with the corresponding NLOS scenarios where the direct wave is blocked by a computer screen.

II. 60 GHz Radio Channel Measurements

The 60 GHz channel was measured in a conference room at Aalto University, Espoo, Finland using a vector network analyzer based system [6]. The measured frequency range was 61-65 GHz, using 2001 frequency points. A 7×7 planar virtual array was used at both the Tx and the Rx side. Using 2-D electromechanical positioners, the Tx and Rx arrays were scanned in the horizontal and vertical planes, respectively. The Tx antenna was a commercial biconical antenna with an omnidirectional pattern in azimuth, while the Rx antenna was an open waveguide. The inter-element spacing was 2 mm in both arrays. The Rx array remained at a fixed location, whereas the Tx array was placed at 17 different positions on top of the tables. A LOS and a NLOS scenario was measured for all positions except for two Tx positions, where only a LOS scenario was measured. The difference between the LOS and NLOS scenarios are made solely by blocking the LOS path

978-1-4244-8331-0/11/$26.00 ©2011 IEEE

with a laptop screen placed 0.42 m away from the Tx. Other objects in the measurement environment and the locations of the arrays were the same for the LOS and NLOS scenarios.

III. Directional analysis

A. Signal Model for the Analysis

The measured channel matrix $\mathbf{H}^{\text{meas}}$ is of size 49×49 where each element $h_{m,n}$ contains the channel frequency transfer function between receive and transmit antenna element number m and n, respectively. The transfer function is assumed to be correctly described by the contributions from a finite number of plane waves as [1]:

$$h_{m,n}\left(k,i,\alpha_l,\tau_l,\Theta_l^{Rx},\Theta_l^{Tx},\nu_l\right) = \tag{1}$$

$$\sum_{l=1}^{L}\alpha_l \mathrm{e}^{-j2\pi\Delta f\tau_l k}G_{Tx}\left(n,k,\Theta_l^{Tx}\right)G_{Rx}(m,k,\Theta_l^{Rx})\,\mathrm{e}^{j2\pi\Delta t\nu_l i},$$

where L is the total number of multipath components (MPCs), α_l, τ_l, Θ_l^{Tx} and Θ_l^{Rx} is the complex amplitude, delay, direction of arrival (DOA) and direction of departure (DOD), respectively. G_{Tx}, G_{Rx} and k is the complex antenna pattern of the Tx and Rx, and frequency sub-index, respectively. Since the channel was measured in a time-static environment with only one snapshot, the Doppler frequency, ν, and the snapshot index, i, can be omitted in (1). In the analysis, an observation bandwidth of 300 MHz around 62 GHz with 26 frequency samples is used.

B. The SAGE Algorithm

The SAGE algorithm [7] is an iterative method for obtaining maximum-likelihood estimates of the MPC parameters. In this paper, the SAGE algorithm is used to provide the directional estimates of the channel as well as estimates of the complex amplitudes and the delay. In these evaluations, 50 MPCs are estimated. In our analysis, we have considered synthetic antenna patterns, i.e., each array element is an omni-directional antennna with a phase shift that depends on the direction of the incoming plane wave and the array geometry. The elevation estimates for the DOD of the l:th MPC, θ_l^{Tx}, have ambiguities due to the horizontal array geometry of the Tx array: it cannot be determined whether they arrive from the upper or lower half-space, whereas the measurement arrangement allows such a determination at the Rx. This ambiguity can be resolved by assuming that no double-reflections (via floor and ceiling) occur; in this case MPCs with a DOA in the upper half-sphere have a DOD that also must lie in the upper half-sphere. Measurement results confirm that very few MPCs exhibit the mentioned double-reflections, and furthermore those MPCs have low power.

C. Reconstruction Error and Residual Power

The signal model in (1) does not cover spherical waves or diffuse multipath components. As a result, the total power of the extracted MPCs are therefore in general lower than the power of the observed signals at the antenna ports. The mean square relative reconstruction error ($MSRRE$) and the relative residual signal power, Λ, were calculated using the estimates given by SAGE for $L = 50$ MPCs, as [8]

$$MSRRE = \frac{1}{K}\sum_{k=1}^{K}\left(\frac{||\mathbf{H}_k^{\text{meas}}-\mathbf{H}(L)_k^{\text{re.}}||_F^2 - P_{\text{n}}}{||\mathbf{H}_k^{\text{meas}}||_F^2 - P_{\text{n}}}\right) \tag{2}$$

$$\Lambda = 1 - \frac{1}{K}\sum_{k=1}^{K}\left(\frac{||\mathbf{H}(L)_k^{\text{re.}}||_F^2}{||\mathbf{H}_k^{\text{meas}}||_F^2 - P_{\text{n}}}\right) \tag{3}$$

Here, $\mathbf{H}^{\text{re.}}$ is the matrix reconstructed by the signal model in (1) using L MPC parameters estimated by SAGE. The summation is over the K different frequency sub-indexes and $||\cdot||_F$ denotes the Frobenius norm. In (3), P_{n} is the estimated noise power from each measurement. The noise power was estimated from a part of the power delay profile where no signals were observed.

The calculated CDFs of the relative residual power and the MSRRE can be seen in figure 1. In the LOS scenario, the residual signal power is less than 7 % for all Tx positions. The residual power in the NLOS scenario is higher, although it is less than 20 % in most cases. The values of the MSRRE are only slightly higher than those of the residual power.

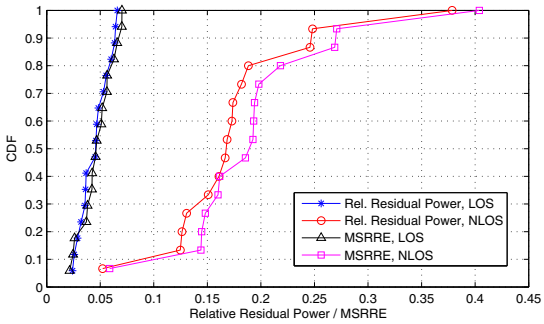

Fig. 1. CDFs of the relative residual power and the MSRRE for the different Tx positions in the LOS and NLOS scenarios.

D. Direction Spread

The direction spread is calculated as [9]

$$\sigma_\Omega = \sqrt{\sum_{l=1}^{L}|e(\phi_l,\theta_l)-\mu_\Omega|^2 P(\phi_l,\theta_l)}, \tag{4}$$

where μ_Ω and the unit vector for the direction of the l:th component, $e(\phi_l,\theta_l)$, are given by

$$\mu_\Omega = \sum_{l=1}^{L} e(\phi_l,\theta_l)P(\phi_l,\theta_l)$$

$$e(\phi_l,\theta_l) = [\cos(\phi_l)\sin(\theta_l),\ \sin(\phi_l)\sin(\theta_l),\ \cos(\theta_l)]^{\text{T}}$$

Here, P is the normalized power spectrum, while ϕ_l and θ_l is the azimuth and elevation angle of the l:th MPC, respectively.

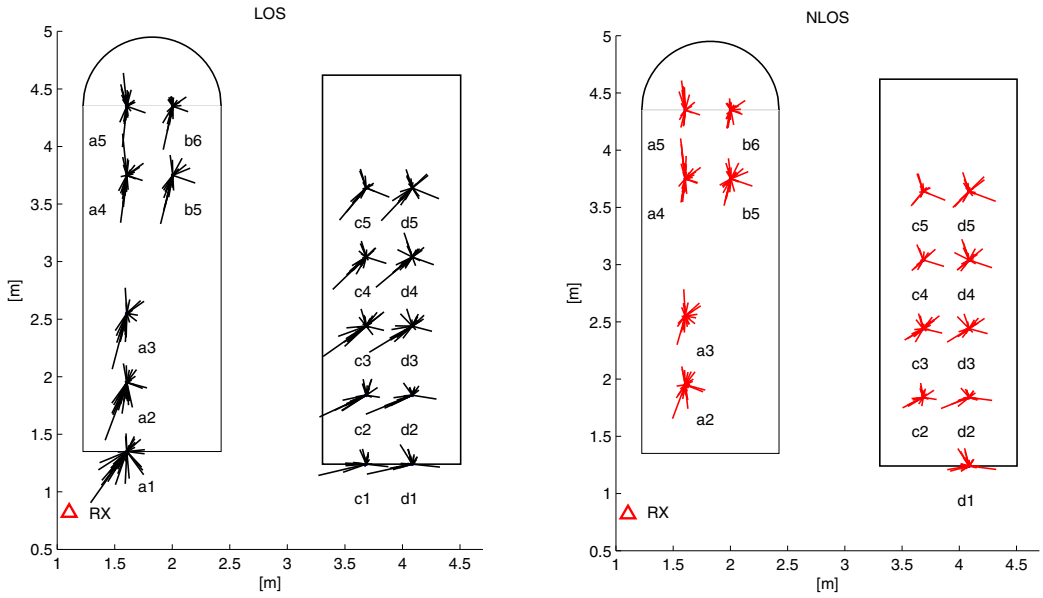

Fig. 2. Tx azimuth estimates for all Tx positions in the LOS and NLOS scenarios. The length of the lines are proportional to the power of each MPC in dB.

IV. Results

A. Directional Estimates

Figure 2 shows the Tx azimuth estimates for all the Tx positions in the LOS and NLOS scenarios. The site map of the conference room where the measurements took place can be seen in figure 3. The length of the lines in figures 2 are proportional to the absolute values of the MPC powers in dB. The power of the direct wave is on the order of 20 dB stronger than the second strongest component for all positions except for positions a4 and a5, where the difference is only 4 dB. When comparing figure 2(a) and 2(b), it becomes evident that the estimates are very similar except in the direction around the direct wave. For all positions in the NLOS scenario, there is a significant component departing in the same azimuth direction as the LOS component in the LOS scenario. When both the elevation and azimuth estimates are taken into account, it is confirmed that these MPCs are diffracted around the top edge of the computer screen. The power of these MPCs is 18-20 dB lower compared to the direct wave in each corresponding LOS scenario. We note that the height difference between the screen and the Tx/Rx is only 7.5 cm.

Figure 3 shows the floorplan with the estimates of the 27 strongest MPCs in the LOS scenario with the Tx in position a3. The black lines are the estimated azimuth DODs and DOAs given by SAGE, while the dashed lines are expected pathways connecting the Tx and the Rx based on geometrical optics. Also shown is the coordinate system that is used as a local coordinate system at both the Tx and the Rx. The azimuth angle, ϕ, and the elevation angle, θ, is defined as shown in figure 3. The vertical receive antenna array is oriented such that the antenna boresight is pointing in the direction $(\phi, \theta) = (320°, 0°)$. There is a large number of components

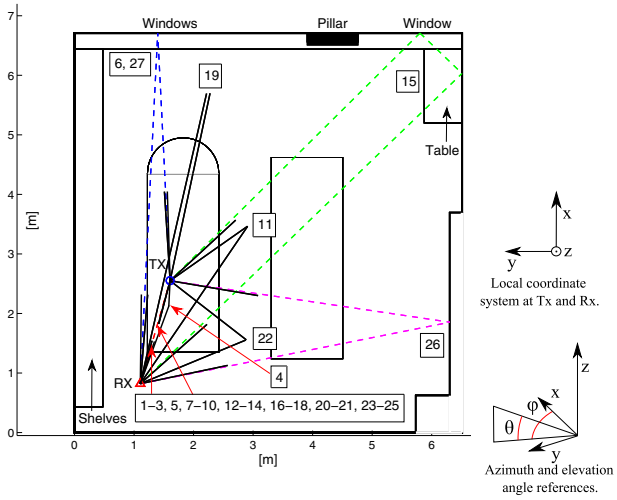

Fig. 3. Floorplan of the meeting room where the measurements took place with the Tx in one of 17 positions. The black lines are the azimuth estimates for the 27 strongest components in the LOS scenario.

centered around the LOS direction. These components could be physically existing MPCs that are created by reflections from the metallic parts of the antenna/waveguide fixtures (even though absorbing materials were placed on the fixtures during the measurements). Some of these components might be artifacts created due to an imperfect subtraction of the LOS component in the successive interference cancellation step in SAGE. This effect could be mitigated by using a complete data model of the antenna patterns.

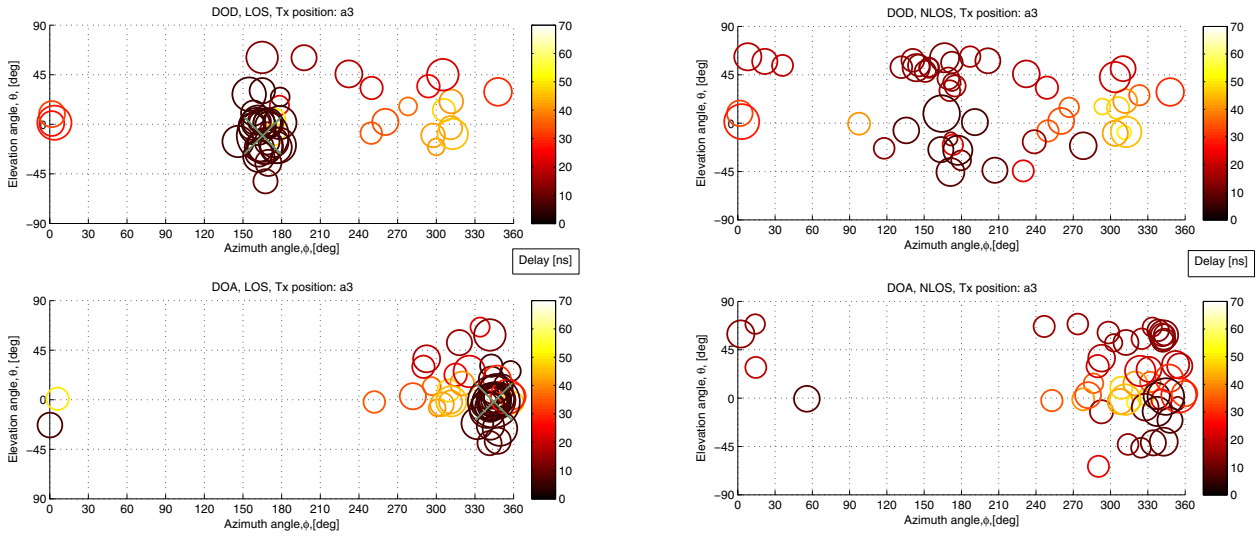

(a) (b)

Fig. 4. Fig. 4. DOD and DOA for the (a) LOS and, (b) NLOS scenarios with the Tx in position a3.

B. Signal Pathways

Table I shows the identified pathways of the components that also are illustrated in Fig. 3. Some of the components appear to be reflected on a window or an object embedded around the window, such as blinds or the frames around the window. One component is reflected on the ceiling and three other components are identified as being reflected on ceiling lamps, which have a metallic cover. This suggests that it is important to include the elevation estimates in the description of the directional properties of the channel.

TABLE I
IDENTIFIED SIGNAL PATHWAYS.

MPC #	Identified signal path	Power [dB]	Delay [ns]
1	Direct wave	-70	7.1
4	Table	-92	7.6
6	Window	-95	28.9
11	Ceiling lamp	-95	22.0
12	Ceiling	-95	13.2
15	Window/wall	-97	45.4
19	Ceiling lamp	-100	30.7
22	Ceiling lamp	-101	18.5
26	Wall	-102	34.0
27	Window	-102	33.0

C. DOD and DOA estimates

Figure 4 shows the DOD and DOA for the LOS and NLOS scenarios with the Tx in position a3. The diameters of the circles are proportional to the power of each MPC in dB and the color of each circle represents delay in ns. Figure 4(b) contains a larger number of estimates with longer delays compared to figure 4(a). This is due to the fact that - given the fixed total number of estimated MPCs - the LOS scenario (which has many components near the LOS) allows to extract fewer weak, long-delayed components.

For this reason, it is difficult to make a fair comparison between the two figures. However, most of the MPCs in the LOS scenario, beside the one close to the LOS direction, can also be identified in the NLOS scenario. This indicates that MPCs that are not close to the LOS direction have similar directional properties. The strongest MPC in this NLOS scenario is identified as being diffracted on the top of the computer screen. Modeling the NLOS scenario based on the LOS data with the LOS component removed, as done in the 802.15.3c model, would lead to significant errors in this case.

Figure 5 is the same as figure 4, but with the Tx in position b6 instead. The LOS and NLOS scenarios appear to be more similar in this case. In this NLOS scenario there are some components that are marked ”computer”, which appear to be reflected on the computer screen and are then reflected on a window. This is one of few scenarios where there are significant components that are reflected on the screen.

D. Direction spread

The calculated CDFs of the direction spread is shown in figure 6. The direction spread at the Rx is lower compared to the Tx, which is due to the fact that the Rx is placed in one of the corners of the conference room. Also, the waveguide antenna elements of the vertical Rx array do not radiate in the backward direction towards this corner. The direction spread of the Tx in the LOS scenario is varying a lot for the different Tx positions. For the two Tx positions a5 and a6, the direction spread is substantially higher than in the remaining positions. In both these positions, there are two strong components (the direct wave and a reflection from a window) that have azimuth estimates that are separated by almost 180 degrees. The components are significantly stronger than the remaining ones and the difference of the estimated power for the two components is about 4 dB. The high direction spread in these two cases is almost entirely attributed to the two strongest

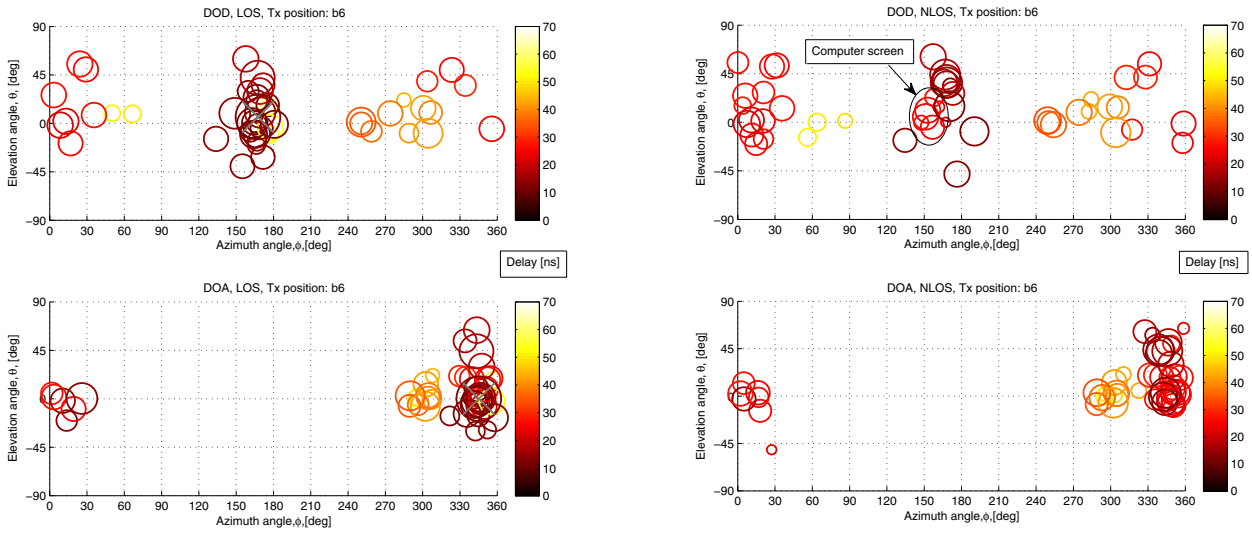

(a) (b)

Fig. 5. Fig. 4. DOD and DOA for the (a) LOS and, (b) NLOS scenarios with the Tx in position b6.

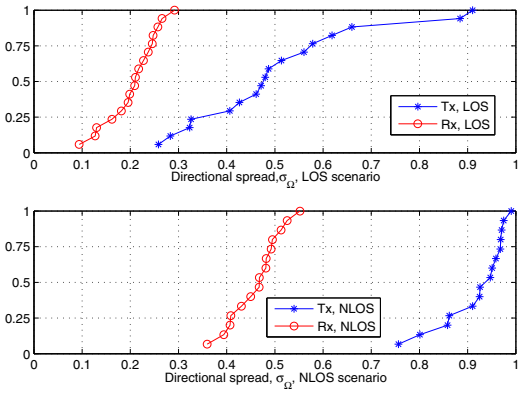

Fig. 6. CDFs of the directional spread for the Tx and the Rx in the LOS and NLOS scenarios.

components. The implication of this is that the direction spread measure should be viewed together with information about the power distribution of the components. In the NLOS scenario, the direction spread for the Tx is above 0.9 for most positions. However, we note that there are few strong reflections present in the NLOS scenario.

V. Conclusions

The 60 GHz radio channel was measured in a conference room and the SAGE algorithm was applied to the measured data to give estimates of the MPC parameters for LOS and NLOS scenarios. It has been shown that it is possible to identify the signal pathways and corresponding scattering objects for different MPCs of the measured 60 GHz radio channel and that the estimates given by SAGE agree well with the geometry of the measurement site. The study also showed that the directional properties of the channel in the LOS and NLOS scenarios are very similar except around the LOS direction. In the NLOS scenario, diffraction around the objects blocking the LOS was shown to be a significant propagation mechanism, giving rise to an insight into the existing channel models that the NLOS channel cannot be realized just by omitting the LOS component. A comparison of the directional estimates with the geometry of the room suggests that it is important to include the elevation estimates in the description of the directional properties of the channel. Direction spread measures for both the Tx and the Rx were presented for both LOS and NLOS scenarios.

References

[1] A. F. Molisch, "Wireless Communications", 2nd edition, *Chicester, U.K, IEEE Press - Wiley*, 2011.

[2] X. An, C.-S. Sum, R.V. Prasad, J. Wang, Z. Lan, J. Wang, R. Hekmat, H. Harada, I. Niemegeers, "Beam switching support to resolve link-blockage problem in 60 GHz WPANs," *Proc. of IEEE Int. Symp. on Personal, Indoor and Mobile Radio Communications*, 2009, Tokyo, Japan.

[3] H. Xu, V. Kukshya and T. S. Rappaport, "Spatial and Temporal Characteristics of 60-GHz indoor Channels", *IEEE Journal on Selected Areas in Communications*, Vol. 20, No. 3, April 2002.

[4] M.-S. Choi, G. Grosskopf and D. Rohde, "Statistical Characteristics of 60 GHz Wideband Indoor Propagation Channel", *Proc. 16th Annual IEEE Int. Symposium on Personal, Indoor and Mobile Radio Comm.*, Berlin, Germany, 2005.

[5] S-K. Yong, *et al.*, "TG3c channel modeling sub-commitee final report", *IEEE Techn. Rep.*,15-07-0584-01-003c, Mar. 2007.

[6] S. Ranvier, M. Kyro, K. Haneda, C. Icheln and P. Vainikainen, "VNA-based wideband 60 GHz MIMO channel sounder with 3D arrays", *Proc. Radio Wireless Symp.* 2009, pp. 308-311, San Diego, CA, Jan 2009.

[7] B. H. Fleury, P. Jourdan, and A. Stucki, "High-resolution channel parameter estimation for MIMO applications using the SAGE algorithm", *Proc. 2002 Int. Zurich Seminar on Broadband Communications - Access, Transmission, Networking*, ETH Zurich, Switzerland, Feb. 2002.

[8] S. Wyne. A. F. Molisch, P. Almers, G. Eriksson, J. Karedal, F. Tufvesson, "Outdoor-to-Indoor Office MIMO Measurements and Analysis at 5.2 GHz", *IEEE Trans. on Vehicular Technology*, Vol. 57 , Issue 3, 2008.

[9] B. H. Fleury, First- and second-order characterization of direction dispersion and space selectivity in the radio channel, *IEEE Transactions on Information Theory*, vol. 46, pp. 2027 - 2044, September 2000.